System Integration and Preliminary Clinical Evaluation of a Robotic System for MRI-Guided Transperineal Prostate Biopsy

Niravkumar A. Patel[a,†,*], **Gang Li**[a,†], **Weijian Shang**[a], **Marek Wartenberg**[a], **Tamas Heffter**[b], **Everette C. Burdette**[b], **Iulian Iordachita**[c], **Junichi Tokuda**[d], **Nobuhiko Hata**[d], **Clare M. Tempany**[d], **Gregory S. Fischer**[a]

[a]Automation and Interventional Medicine Laboratory, Worcester Polytechnic Institute, Worcester, MA 01609, USA [napatel, gfischerj]@wpi.edu

[b]Acoustic MedSystems Inc., Savoy, IL, USA.

[c]Laboratory for Computational Sensing and Robotics (LCSR), Johns Hopkins University, Baltimore, MD, USA.

[d]Department of Radiology, Surgical Navigation and Robotics Laboratory, Brigham and Womens Hospital, Harvard Medical School, Boston, MA, USA.

[†] indicates shared first authorship.

Abstract

This paper presents the development, preclinical evaluation, and preliminary clinical study of a robotic system for targeted transperineal prostate biopsy under direct interventional magnetic resonance imaging (MRI) guidance. The clinically integrated robotic system is developed based on a modular design approach, comprised of surgical navigation application, robot control software, MRI robot controller hardware, and robotic needle placement manipulator. The system provides enabling technologies for MRI-guided procedures. It can be easily transported and setup for supporting the clinical workflow of interventional procedures, and the system is readily extensible and reconfigurable to other clinical applications. Preclinical evaluation of the system is performed with phantom studies in a 3 Tesla MRI scanner, rehearsing the proposed clinical workflow, and demonstrating an in-plane targeting error of 1.5mm. The robotic system has been approved by the institutional review board (IRB) for clinical trials. A preliminary clinical study is conducted with the patient consent, demonstrating the targeting errors at two biopsy target sites to be $4.0mm$ and $3.7mm$, which is sufficient to target a clinically significant tumor foci. First-in-human trials to evaluate the system's effectiveness and accuracy for MR image-guide prostate biopsy are underway.

Keywords

MRI-guided prostate biopsy; MRI-compatible robotic system; piezoelectric actuation; image-guided surgery

---

[*]indicates corresponding author.

1. Introduction

Prostate cancer is the second most common cancer and the second leading cause of cancer death in American men. According to the American Cancer Society, about 1 in 7 men will be diagnosed with prostate cancer and 1 in 38 will die of prostate cancer. Image-guided therapy (IGT) offers improved diagnosis and therapy for prostate cancer, thanks to its capabilities for providing intraoperative image-based feedback enabling greater procedural accuracy. Transrectal ultrasound (TRUS) is the current standard of care imaging modality for guiding prostate biopsy and brachytherapy seed placement, but the relatively low image quality can only offer minimal specific information of the prostate tumor, which limits its ability to precisely localize suspicious focal lesions.[1,2] MRI is an alternative and ideal modality for surgical guidance due to its ability to perform multi- parametric and high resolution soft tissue imaging without ionizing radiation.[3] TRUS-MRI fusion is an approach, where previously acquired MRI images are registered to ultrasound images during the biopsy procedure.[4] This approach has shown increased cancer detection rate compared to untargeted methods,[5,6] however this approach relies on MR-US image registration to preoperative MRI and does not utilized interactively updated intraoperative MR images. Manually operated devices have been utilized to guide needle placement inside an MRI scanner[7-10] to utilize intraoperative MR images. However, the tightly confined scanner bore (typically 60 — 70cm in diameter) restricts the accessible space and results in awkward ergonomics for accurately placing needles inside the MRI machine. To address this issue, robotic devices have been introduced into the MRI-guided procedures for assisting needle placement.

Challenges of developing a robotic systems that operate in the MRI environment include the strong magnetic (usually 1.5T to 3T) and radio frequency (RF) fields. Such a stringent environment poses potential safety hazards, due to which the American Society for Testing and Materials (ASTM) classified the devices for the MRI environment as MRI-Safe, MRI-Conditional and MRI-Unsafe (ASTM F2503). Significant efforts have been investigated to overcome these critical issues for MRI-compatible robotic systems.

Pneumatics and piezoelectrics are the two commonly utilized actuation methods in an MRI environment. Various research groups have developed pneumatically actuated MRI robotic systems based on pneumatic cylin- ders.[11-14] Also, custom pneumatic stepping actuators have been adopted for prostate interventions.[15-17] Schouten et al. presented a pneumatic turbine-based actuator.[18]. A servo-pneumatic drive system developed by Innomotion (Innomedic, Herxheim, Germany) was applied to the first cadaver study of transgluteal biopsies, and then tested clinically in patients.[19]

Although the fundamental principle of pneumatic actuation can be MRI-safe, nonmagnetic piezoelectric actuators are able to provide high precision positioning (submicron) with excellent dynamic performance. Moreover, they can be made compact in size with high power density. Song et al. presented a 2-DOF motorized needle guide template with piezoelectric ultrasonic motors to resemble the conventional TRUS-guided prostate intervention.[20] Krieger et al. designed a compact prototype of piezoelectrically actuated robot for transrectal MRI-guided needle intervention with 2-DOF motorized needle driver

mounted on a 6-DOF passive arm.[21] Nevertheless, significant image degradation is a major problem for piezoelectric actuators that utilize commercially available off-the-shelf drive electronics. The signal-to-noise ratio (SNR) of MR images may be reduced by as much as 80% without RF shielding, and even with RF shielding the SNR may still be degraded by 40% - 60%.[21,22] In our previous work, we have developed a custom MRI robot controller to drive piezoelectric actuators,[23] which demonstrates that SNR reduction can be limited to 15%.[24,25]

Although several MRI-guided robotic systems have demonstrated feasibility of performing interventional procedures in phantom studies, only very few of them have been tested clinically. Transperineal[26,27], transrectal[7,28] and transgluteal[19] approaches have been tested clinically for MRI-guided prostate biopsy procedures. Further development and thorough clinical certification are required to advance for clinical use, especially from the perspective of targeting accuracy, clinical workflow, safety mechanisms and sterilization. A comprehensive review of MRI-guided robotics and corresponding actuation methods have been presented.[29-31]

In this paper, we present the development, preclinical evaluation, and a preliminary patient trial of a clinically integrated robotic system for interventional MRI-guided transperineal prostate biopsy. This robotic system has been approved by the institutional review board (IRB) for clinical trials, and clinical studies are ongoing in the Advanced Multimodality Image Guided Operating (AMIGO) suite at Brigham and Womens Hospital (BWH). This clinical iteration of the robotic system is built upon our previously developed family of prototype versions.[32,33] In this study, we are adopting the latest version of a parallel manipulator with piezoelectrically actuated needle alignment and manual insertion,[33] and incorporating it into a complete clinical image-guided surgery system. The custom developed MRI robot controller hardware[24] is modified to drive the ultrasonic piezoelectric motors, and further enhanced for reliability and safety, making it suitable for clinical use. The primary contributions of this study are: 1) development of a complete clinically integrated robotic system, which has been approved by IRB for clinical trials; 2) preclinical evaluation with MRI phantom studies, validating the system targeting accuracy and clinical workflow; 3) demonstration of clinical application with a preliminary patient study.

2. Material And Methods

2.1. System Architecture

This system is developed to improve the conventional MRI-guided prostate biopsy procedure by augmenting the manual procedure with a robotic needle alignment device. Though optimized for prostate biopsy procedures, it adopts a modular design approach making the architecture capable of supporting various needle-based interventional procedures. The system comprises four major modules: 1) surgical planning and navigation application, 2) robot control software, 3) robot controller, and 4) robotic needle placement manipulator. In the beginning of the procedure, 3D- Slicer[34] is used to prepare the surgical plan by registering the intraoperative images to the preoperative planning images based on the deformable registration method.[35] Targets defined in the intraoperative images are transferred to the surgical navigation application RadVision® (Acoustic MedSystems Inc.,

IL, USA), which visualizes the targets in image space, registers the robot's coordinate frame to the MR images, and forwards the registered targets to the robot control software via OpenIGTLink communication protocol.[36]

The robot control software computes the robot's inverse kinematics and motion control plan, resolving the targets from task space (patient coordinates) to joint space (robot motions) and ensures that the desired target is reachable. The custom MRI robot controller is developed to provide high precision and low noise closed-loop control of the ultrasonic piezoelectric motors. The connection between the robot control software (running on a computer in the console room) and the robot controller (residing beside the MRI scanner)is established through Fiberoptic Ether-net, which is run through the patch panel of the MRI scanner room to eliminate the transmission of any electrical signals which may introduce noise during imaging. Fig. 1 illustrates the clinical system configuration, distinguishing the components inside the MRI scanner room and the control console room, while Fig. 2 shows system components and data flow between them.

Safety and reliability are crucial design considerations for a robotic system used in a clinical environment, and thus a key contribution of this work is producing a clinically viable robotic assistant. To this end, several safety mechanisms are introduced into the improved controller design. A non-metallic foot pedal equipped with a fiberoptic photoelectric sensor is utilized by the clinician as an interlock for enabling motion only when engaged. This interlock interacts directly with the lowest level motion control modules in the controller, and is therefore independent of any high level software. Custom optical limit switches are installed on both ends of the four sliders to prevent damaging the robot when reaching hard stops at the edge of the mechanism, and also serve as a reliable means for initializing the robot's home position. Fiber-coupled LED indicators mounted on the upper surface of the controller box indicate the status of each piezoelectric driver module. Stall detection based on the encoder feedback is used to monitor the robot motion status. In case a malfunction is detected (e.g. encoder reading lost, jumped, or updated incorrectly), the stall detection mechanism automatically triggers a solid state relay on the backplane that disconnects motor power to the motion control modules and stops the robot motion. In case of any urgent robot failure, an emergency-stop switch installed in the power chain between the $24\,V$ regulator and the motor drivers can be pressed by an user to shut down the motor power.

2.2 Clinical Workflow

The clinical workflow of the proposed robot-assisted procedure is intended to mimic that of the template-based prostate interventions,[37] allowing similar location of surgical personnel and use of standard equipment. Fig. 3 illustrates the clinical workflow comparison of template-based and robotic approach, wherein the times per stage are compared; it should be noted that, there is significant improvement in needle alignment time with the robotic procedure, which is typically repeated a number of times for a given procedure. The workflow steps for the robotic approach are as follows:

(1) Place patient support board inside MRI scanner bore, position patient on the board in semi-lithotomy position.

(2)   Image the fiducial frame (attached to patient board near the patient's perenium) and the prostate of patient.

(3)   Register the robot to image space (i.e. patient coordinates) based upon fiducial frame images.

(4)   Register intraoperative images to preoperative images and define/confirm the targets.

(5)   Initialize the robot outside the scanner bore.

(6)   Cover the robot with sterile drape and attach the sterile needle guide.

(7)   Slide the robot into guides on the patient board and lock in place.

(8)   Set a target in image space using the navigation user interface.

(9)   Align the robot automatically and insert the needle manually along defined trajectory.

(10)   Take confirmation images to verify needle tip position.

(11)   If needle is not at desired target position, retract the needle and jump to step 9

(12)   Collect biopsy sample and retract the needle manually.

(13)   Repeat steps 8 — 11 for each suspected lesion.

The patient preparation process, which includes patient positioning, anesthesia, and configuring the sterile field matches the conventional template-based procedures, helping ensure a level of comfort among the clinical team with the use of the robotic device. As shown in Fig. 4, the robotic system ensures that the workflow are secure and maintained, allowing only validated state transitions to pass through. Invalid transitions (e.g. sending target without a valid registration) are not performed and reported to the user. Once the robotic manipulator is aligned (with motion only occurring while a footpedal interlock is asserted), the actuators are isolated from the power source resulting in a self-brake state to prevent any unintentional motion during the needle insertion stage. MR images are acquired after the needle is inserted to confirm that it is aligned to the target. At that point, the physician makes a decision on whether to collect the biopsy sample or perform a trajectory correction operation.

The robotic system is able to improve upon the procedure as compared to a template-based device, especially with regard to targeting accuracy, procedure time, and ergonomics. The template-based approach utilizes a needle guidance template consisting of a grid of holes spaced 5mm apart. In contrast, the robotic manipulator could be controlled to set the needle insertion hole with a resolution of better than 0.01mm. It is not uncommon in clinical procedures for adjustments to be required in cases where the initial insertion attempt is not acceptable. In the template- based approaches, adjustments are often conducted by inserting the needle through a neighboring guidance hole from the initial one, which is typically 5mm apart. The robotic system enables finer needle placement adjustments. Also, it offers the ability to angulate the needle guide which makes it possible to guide insertion of the needle at oblique angles, which is useful to avoid pubic arch interference. The robotic system

eliminates the need for mental computation of the coordinates and alignment of insertion holes for each insertion attempt, which is prone to human error. Hence, the procedure duration could be potentially reduced up to 55 min for single insertion, especially in cases where multiple insertion attempts are performed.

2.3 Needle Placement Manipulator

The robotic manipulator used in this system is designed to perform in-bore transperineal prostate interventions with the patient lying in the supine position and legs in the semi-lithotomy configuration. To cover the entire prostate volume and accommodate patient variability, the manipulator is designed to provide 4-DOF actuated motion (2-DOF translation and 2-DOF angulation) for aligning the needle with two trapezoid stages, as shown in Fig. 5. The linear sliders of the trapezoid stages are driven by an ultrasonic piezoelectric motor (USR60-S4N, Shinsei Corp., Tokyo, Japan). A needle guide is attached on top of the trapezoid stages for guiding the needle insertion trajectory.

The manipulator platform is slid into the patient board via two linear rails and is locked in place with thumb screws. The sterile fiducial frame comprises nine embedded MRI- visible fluid tubes (MR-Spots, Beekley Corp., Bristol, CT), which are configured in three sets of "Z" shapes in three orthogonal planes. The fiducial frame((referred to as Z- Frame) can be repeatably fixed on the centerline of the patient board, and also serves to constrain the skin of the patient's perineum and maintain the robot's workspace between the patient's legs.

The manipulator is manufactured from MRI compatible materials. The needle guide and fiducial frame, which have direct contact with patient and needs to be sterilized, are 3D printed with biocompatible Ultem (Polyether- imide) and Polycarbonate, respectively. The sterile components have been certified by Nelson Labs (Salt Lake City, UT) for sterilization using Sterrad 100S system (Advanced Sterilization Products, Irvine, CA). All the other components of the manipulator are covered with a disposable, pre-sterilized clinical plastic drape to create the sterile environment. Detailed descriptions of mechanism design, robot kinematics, and workspace analysis were presented in our previous work.[33]

2.4 Piezoelectric Actuation and Control

Piezoelectric actuators are driven by the controlled oscillation of ceramic crystals based on the piezoelectric effect. The Shinsei harmonic ultrasonic actuator is adopted in this robotic system, due to its unique characteristics of high torque output, self-retention, and compactness. A custom MRI robot controller[24] was adapted for this robotic system with appropriate modifications and improvements to drive Shinsei motors and control the robot. The controller consists of two primary components within a shielded enclosure: 1) The backplane which includes an embedded microcontroller that coordinates the motion control information from the planning level to the device level and 2) piezoelectric driver modules which generate control signals and perform closed loop motion control of the ultrasonic motors. Also, to minimize electromagentic interference (EMI) emissions from the controller, linear power supplies, fiberoptic communications, low noise elctronics with electrical filtering, and shielding including enclosing the system in an aluminium enclosure with integrated wave guides are used.

2.5. Image-Based Robot Registration and Surgical Navigation

The surgical plan is prepared by selecting targets at suspected lesions using co-registered multi-parametric preoperative images which are pushed to the 3D Slicer workstation from the scanner console over network communication established using TCP/IP socket. At the start of the procedure, intraoperative images are acquired and deformable registration is performed using 3D Slicer to relate the surgical plan from preoperative images to intraoperative images. The registered surgical plan(i.e target in patient coordinate system/MR image space in right-anterior- superior (RAS) coordinates) are transferred to the navigation software RadVision using a USB memory stick, where they are displayed to the clinician for visual confirmation. Fig. 6 illustrates the RadVision user interface, which is configured for this study to perform fiducial frame registration, surgical navigation, and supervisory control of the robot.

Fiducial frame-based registration is performed to register the robot to the patient coordinate system. Scans of the fiducial frame are performed and the DICOM images are pushed to RadVision from the scanner console over network communication established using TCP/IP socket, which then calculates the robot registration transform using line marker registration which has reported a registration accuracy of 1.00 ± 0.73 mm and 1.41 ± 1.06 degrees.[38] The calculated registration transform is then sent to the robot control software via OpenIGTLink, where it is used to calculate the 6-DOF needle tip pose in patient coordinates through the transformation chain as shown in Fig. 7; calculated 6-DOF needle tip pose is used to perform robotic positioning and alignment of insertion axis, with insertion and rotation performed manually along that axis. T_{RAS}^{Z} is the transform from the scanner coordinate system to the Z-Frame origin, while T_{Base}^{Z} is the transform from the Z-Frame origin to robot base and T_{Tip}^{Base} is the transform from robot base to the needle tip, which is calculated using robots kinematics giving needle tip in robot coordinate system. The needle tip pose in scanner coordinate system T_{Base}^{Tip} is calculated using Eq. (1).

$$T_{Tip}^{RAS} = T_{Z}^{RAS} * T_{Base}^{Z} * T_{Tip}^{Base} \quad 1$$

The patient anatomy is visualized in RadVision in the axial, sagittal and coronal perspectives, as well as a combined 3D view for monitoring the needle track and confirming actual target positions. During the procedure, targets defined in patient coordinates at the time of surgical planning are selected in RadVision, and then sent to the robot control software. On receiving the desired target transform (i.e. tip position and needle trajectory), the robot control application calculates desired joint positions using robot registration transform and inverse kinematics of the manipulator. Target positions for each joint of the robot are finally sent to the robot controller via the Bowler communication protocol(Neuron Robotics, MA, USA), and the robot awaits foot pedal engagement by the clinician to initiate motion.

The robot control software is developed with the capability to: define robot description using extensible markup language (XML), compute forward and inverse kinematics, evaluate/confirm the reachable workspace, generate coordinated joint motion commands, communicate using OpenIGTLink, and provide user interfaces for clinicians and system operating engineers. The clinical workflow is controlled by an underlying state machine allowing only appropriate transitions. The robot control application ensures the clinical workflow by coordinated communication with robot controller and the navigation software.

3. Results

In this study, we focus on the preclinical evaluation of the system with validation through phantom studies under MRI guidance and a clinical feasibility with preliminary patient study. A primary contribution of this work is to validate the readiness of the newly developed system for scaled up clinical trials.

3.1. Preclinical Evaluation

Phantom studies were performed under live MRI guidance to evaluate the targeting accuracy of the system inside a 3T MAGNETOM Verio scanner (Siemens AG, Erlangen, Germany). The phantom used in this study is a mixture of gelatin(Knox, Kraft Foods, Northfield, IL, USA) and water with 22% concentration. An 18-gauge MRI-Conditional biopsy needle(Invivo, Gainesville, FL, USA) was manually inserted into the phantom along the robotically aligned trajectory and imaged with diagnostic T2-weighted turbo spin echo (T2W-TSE) imaging protocol (imaging parameters are listed in Table 2: Needle Confirmation). The experiment was conducted in five independent sessions. For each session, new registration of the fiducial frame and initialization of the robot were performed, and five targets were randomly selected in RadVision covering typical focal region of prostate biopsy. Hence, 25 targets in total were collected to assess the system accuracy. The experimental setup was designed as a mockup of typical clinical procedures, which commonly include 1 — 5 targets and require only one registration for each patient. The experiment was conducted with the clinical team and strictly followed the proposed clinical workflow shown in Fig. 3.

The desired target positions defined in RadVision were compared with actual needle tip positions (manually segmented from MRI volume images) to assess targeting accuracy. For the clinical procedures, the in-plane (RA-plane) error plays more a significant role than the error along the needle insertion axis (S-axis), since the insertion depth along S-axis is adjusted manually by the clinician to the desired depth via interactively updated intraoperative MR imaging (iMRI). Therefore, in-plane error is the primary metric assessed in this study, with results depicted in Fig. 8. The experiment results are summarized for each of the five sessions in Table 1, with RMS error in the R-axis (signed lateral), A-axis (signed vertical), and RA-plane (total magnitude) of $1.1mm$, $1.0mm$, and $1.5mm$, respectively.

3.2. Preliminary Clinical Patient Study

This paper reports viability of the presented approach through a clinical procedure of prostate biopsy performed on a 60 year old male patient inside a 3T MAGNETOM Verio

scanner. The study was approved by an IRB, patient consent was obtained (the patient did not have to bear any additional cost for getting the procedure with the robotic device assistance), and the aforementioned clinical workflow was strictly followed. Under intravenous conscious sedation, the patient was placed on the patient board in the semi-lithotomy position with legs rested on the supports. For this patient study, the system configuration is illustrated in Fig. 9, and the imaging protocols are listed in Table 2. After patient positioning and preparation, the sterilized fiducial frame was attached on the patient board and registration was performed by acquiring MRI images with the *Localizer* protocol. After registering the fiducial frame, a new set of images of the prostate region were acquired using the *Intraoperative* protocol with Body Matrix and Spine Matrix coils (Siemens AG, Erlangen, Germany). Using 3DSlicer, two suspicious sites were identified from previously acquired multi-parametric images and then registered to the intraoperative anatomical images. Registered plan consisting of identified targets was transferred to RadVision over the network and then sent to the controller for aligning the robot manipulator. Once the robot was aligned in place, the radiologist reached in the scanner bore and manually inserted an 18-gauge MRI-Conditional core biopsy needle (Fully Automatic Biopsy Gun, Invivo, Gainesville, FL, USA) into the prostate gland through the robotically aligned needle guide. A confirmation image set was used to validate the actual needle tip location with the *Needle Confirmation* protocol. If the needle were not within the target lesion, adjustments (reinsertion and reorientation) were performed manually by the clinician. Once the needle was confirmed to be in the target, a biopsy sample was manually procured and then the second lesion was targeted in the same manner. For both targets LCGApex and RPZMid(Table. 3), physician performed 4 needle insertions and collected 3 and 1 biopsy samples, respectively. Fig. 10 shows the segmented actual needle trajectories overlaid on a 3D view showing an MRI image of the prostate gland and defined targets.

The targeting accuracy of the biopsy was evaluated by computing the shortest distance from the desired target to the actual needle trajectory which represents the error from the robotically aligned needle axis to the target. The slice thickness for the confirmation images were 3mm, so the distance to the needle axis was selected by finding the nearest image slice to the target. Results from the clinical study are summarized in Table 3. The accuracy of first insertion attempt was obtained solely by the robotically aligned needle guide, no adjustment was performed. The accuracy of the best insertion attempt was achieved by physician-directed adjustment techniques(needle guide repositioning, partial/full needle reinsertion and/or needle rotation), which represents a realistic accuracy for actual tissue sampling. The accuracy of the best insertion attempt for the two biopsies were 4.0mm and 3.7*mm*, respectively. This preliminary measure of targeting accuracy is comparable to our previous study on template-based manual (6.05*mm*) and robotic (5.42*mm*) transperineal approach.[27] The total procedure time was 87*min,* which is significantly reduced compared to our previous study on manual (151.29 ± 37.88*mm*) and robotic needle-guidance template (141.67 ± 19.47*mm*).[27] Further, the duration for the portion of the procedure where the two biopsy samples were acquired was only 19mm with the current robotic approach.

4. Discussion

In this study, we report the development of a fully integrated robotic system for MRI-guided transperineal prostate biopsy, which has been approved by IRB for clinical trials. The clinically oriented robotic system described herein is developed based on a modular approach, with the modules connected through a network[15,39]. A major merit of network based modular design is that each module can be developed and tested individually, making it readily configured for supporting a specific clinical workflow and extensible to various clinical applications. The presented modular system architecture has also been applied to realtime MRI guided needle steering,[40] MRI guided stereotactic neurosurgery[23] and MRI guided concentric tube continuum robot.[41]

Safety is a crucial requirement for clinical systems; therefore safety mechanisms were considered during the design phases, which included motion range limit switches, user controlled foot pedal interlock, independent emergency stop power switch, as well as controller status monitoring with hardware and software. The presented integrated system system was found to be a Non-significant Risk device by the IRB, as it met regulatory requirements set forth in Code of Federal Regulations Title 21 812.2(b).[42] All the component in the robot are nonmagnetic; the motor housings are aluminum and covered in plastic enclosures and all the conductive cables carrying control signals are also wrapped in a plastic cover; none of these conductive components come in contact with the patient body during entire operation of the system, and are intentionally designed to be as distal as possible from the operating site. All the robotic components were found to be safe in static magnetic field(3 Tesla), switched gradient magnetic fields and the radio frequency fields, this led to the robot being classified as an MR Conditional device. As the presented robotic system is not an implantable device and is specifically designed to avoid contact or close proximity of any conductive materials to the patient, ASTM tests such as ASTM F2213-06(torque measurements) and ASTM F2182(RF heating) were not performed. Also proper labeling indicating the device classification was ensured. Along with safety, sterility is a unique and critical requirement for clinical devices; for this reason the robot manipulator is designed with non-sterilizable and sterilizable components. Non-sterilizable components are covered by a standard disposable pre-sterilized drape and sterilizable components are prepared in a kit and sterilized prior to the procedure.

In our previous study on the mechanism design,[33] the system's targeting repeatability and accuracy were assessed in free space, demonstrating errors of less than 1mm. In this work, preclinical phantom studies were performed to evaluate the system's targeting accuracy and to rehearse the clinical workflow. The in-plane errors were assessed, indicating an RMS error of $1.5mm$ and maximum error of $2.1mm$. The placement accuracy achieved herein is comparable to other preclinical studies of MRI-guided robotic systems: Stoianovici et al. reported an MRI-safe robot for en-dorectal prostate biopsy with in-vitro targeting accuracy of $2.1mm$,[15] Krieger et al. presented in-plane target accuracy of $2.4mm$ by an actuated transrectal prostate robot.[21] Also Xu et al. reported an accuracy of 2.4±1.2 mm for TRUS-MRI fusion biopsy procedure in phantom studies, however quantifying the targeting accuracy of fusion approach is difficult as the targets are defined in the MR images and verified in ultrasound images. The targeting accuracy of the proposed system reflects the

overall accuracy of the system, which could be classified as registration error (fiducial frame registration and alignment:1.00 ± 0.73 mm[38]), robot manipulator error (robot mechanism backlash, motion control precision:0.73 mm[33]), imager error (imaging resolution:0.7 mm), and un-modeled error (needle deflection as inserting into the phantom). Based on the systematic error depicted in Fig. 8 for each session, it appears that the dominant error source is most likely registration error. To separate robot accuracy from registration accuracy, the mean error is subtracted for each session, resulting in an in-plane RMS error of $0.2 mm$.

A preliminary clinical study was described to demonstrate the clinical viability of this robotic system. The patient study was performed following the IRB approved clinical workflow. The clinical procedure was performed successfully in under 90min, which is a significant reduction in procedure time as compared to our previous study reporting an average procedure time of 147 minutes with manual and robotic needle-guidance template.[27] Two suspicious sites were targeted and one biopsy tissue core was procured from each target site. The maximum targeting error was 4.0mm, which is acceptable to target a clinically significant tumor foci with a sphere of radius $5 mm$.[43] More extensive clinical cases are currently ongoing at BWH, and further thorough accuracy analysis in the aspects of organ motion and needle deflection will be considered in future studies.

Manual needle insertion and tissue biopsy sampling along a robotically aligned axis was adopted in this version of the robotic system as an initial goal, primarily due to safety and clinical acceptability. However, manual operation inside the tightly constrained scanner bore is still ergonomically awkward and time consuming. Future work will focus on implementing clinically viable teleoperated needle placement[44] with a motorized needle driver[45] under real-time needle tip tracking.[40]

5. Conclusions

This paper presented an MRI guided robotic system for targeted transperineal prostate biopsy which has been demonstrated in a preliminary clinical study. The integrated system comprised of surgical planning and navigation applications, robot control application, 4-DOF robotic manipulator compatible with the MRI environment and an associated custom-built modular robot controller; integration of all system components and surgical workflow were presented. Moreover, compatibility with the MRI environment was evaluated in a 3T MRI scanner with varying robot configurations, showing an SNR reduction of 15.35% when the controller is powered on. The presented integrated system was validated with gelatin phantom experiments and reported an in-plane RMS error of $1.5 mm$ and maximum error of $2.1 mm$. The robotic system presented herein was approved by the IRB for clinical trial and was used for a preliminary patient study demonstrating the best attempt targeting errors at two biopsy target sites to be $4.0 mm$ and $3.7 mm$. Though accuracy reported in gelatin phantom experiments is sufficient for targeting clinically significant tumor foci, accuracy of the system in clinical trial could be improved by eliminating error sources such as robot mechanism errors, robot registration errors, errors from needle deflections and patient movement. Future work will focus on development of robotic system for fully actuated biopsy procedure with closed-loop needle steering under real-time MRI guidance to compensate for errors from needle deflection and patient movement.

Acknowledgments

Nomenclature

RAS	Right(+X Axis) - Anterior(+Y Axis) - Superior(+Z Axis) MRI scanner coordinate system
T_{RAS}^{Tip}	Needle tip pose in scanner coordinate system
T_{RAS}^{Z}	Transform from the scanner coordinate system to the Z-Frame origin
T_{Z}^{Base}	Transform from the Z-Frame origin to robot base
T_{Base}^{Tip}	Transform from robot base to the needle Tip
R - A Plane	Plane perpendicular to the needle trajectory
T2W — TSE	T2 weighted turbo Spin Echo
TR	Repetition time
TE	Echo time

Biography

Niravkumar A. Patel received his Bachelors degree in Computer Engineering in 2005 from North Gujarat University, India and M.Tech. degree in Computer Science and Engineering in 2007 from Nirma University, India. He is currently a Doctoral Candidate in the Robotics Engineering program at Worcester Polytechnic Institute, Worcester, MA. His research interests include medical robotics, percutaneous interventions under real-time MRI guidance, needle steering and path planning.

Gang Li received the B.S. degree and M.S. degree in Mechanical Engineering from Harbin Institute of Technology, Harbin, China, in 2008 and 2011, respectively. He received the Ph.D. degree in Mechanical Engineering from Worcester Polytechnic Institute in 2016.

Currently, he is with the General Motors Global R&D Center. His research interests include medical robotics, electromechanical design, MRI-guided percutaneous intervention, and industrial robotics. He received the Link Foundation Fellowship in 2015.


Weijian Shang received his B.S. degree in Precision Instruments and Mechanology from Tsinghua University in Beijing, China in 2009. He also received his M.S. degree in Mechanical Engineering from Worcester Polytechnic Institute in 2012. He received his Ph.D. degree in Mechanical Engineering from Worcester Polytechnic Institute in 2015. He is currently a Research Fellow at Brigham and Women's Hospital and Harvard Medical School.

Marek Wartenberg received his B.S. rolled in a Trans-Atlantic Dual-M.S. partnership, receiving simultaneous M.S. degrees in 2013 from The University of Connecticut and Politecnico di Milano, Milan, Italy in Biomedical Engineering and Automation and Control Engineering, respectively. Marek is currently a Doctoral Candidate in the Robotics Engineering Program at Worcester Polytechnic Institute, Worcester, MA where his research interests include haptics and teleoperation of medical robotic systems under MRI image-guidance.

Tamas Heffter is a senior software engi-neer at Acoustic MedSystems, Inc. His main interest is developing high-quality software components with agile techniques for image guided systems and medical information technologies.
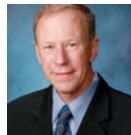
Everentte C. Burdette received the B.S degree in physics, M.S degree in Electrical and Electronics Engineering from Georgia Institute of Technology, and Ph.D. degree in Physiology from Emory University School of Medicine. He is the President and CEO of

Acoustic MedSystems, Inc., a company developing image-guided interventions for brachytherapy, biopsy, surgery, and localized therapies using high intensity ultrasound.

Iulian Iordachita (IEEE M'08, S'14) received the B.Eng. degree in mechanical engineering, the M.Eng. degree in industrial robots, and the Ph.D. degree in mechanical engineering in 1984, 1989, and 1996, respectively, all from the University of Craiova, Craiova, Romania. He is currently an Associate Research Professor at the Laboratory for Computational Sensing and Robotics, Johns Hopkins University, Baltimore, MD, where he is engaged in research on robotics, in particular, robotic hardware. His current research interests include design and manufacturing of surgical instrumentation and devices, medical robots, and mechanisms and mechanical transmissions for robots.

Junichi Tokuda received the B.S. degree in engineering, -the M.S. degree in information science and technology, and the Ph.D. degree in information science and technology in 2002, 2004, and 2007, respectively, all from the University of Tokyo, Tokyo, Japan. He is currently an Assistant Professor of Radiology at Brigham and Women's Hospital and Harvard Medical School, Boston, MA.

Nobuhiko Hata received the B.E. degree in precision machinery engineering in 1993, and the M.E. and D.Eng. degrees in precision machinery engineering in 1995 and 1998, respectively, all from the University of Tokyo, Tokyo, Japan. He is currently an Associate Professor of Radiology at Harvard Medical School, Boston, MA.

Clare M. Tempany received the MB BAO, BCH degrees from the Royal College of Surgeons, Ireland. She is currently the Ferenc Jolesz Chair and the Vice-Chair of Radiology Research, Department of Radiology, Brigham and Women's Hospital, Boston, and a Professor of Radiology at Harvard Medical School. She is also the Clinical Director of the National Image Guided Therapy Center.

Gregory Fischer PhD is an Associate Professor of Mechanical Engineering with appointments in Biomedical Engineering and Robotics Engineering at Worcester Polytechnic Institute. He received B.S. degrees in Electrical Engineering and Mechanical Engineering from Rensselaer Polytechnic Institute, Troy, NY, in 2002 and an M.S.E. degree in Electrical Engineering from Johns Hopkins University, Baltimore, MD, in 2004. He received his Ph.D. degree in Mechanical Engineering from The Johns Hopkins University in 2008. Dr. Fischer is Director of the WPI Automation and Interventional Medicine Laboratory, where his research interests include development of robotic systems for image-guided surgery, haptics and teleoperation, robot mechanism design, surgical device instrumentation, and MRI-compatible robotic systems.

References

References

[1]. Kelloff GJ, Choyke P and Coffey DS, Challenges in clinical prostate cancer: role of imaging AJR., American journal of roentgenology 192(6) (2009) p. 1455. [PubMed: 19457806]

[2]. Han M, Chang D, Kim C, Lee BJ, Zuo Y, Kim H-J, Petrisor D, Trock B, Partin AW, Rodriguez R et al., Geometric evaluation of systematic transrectal ultrasound guided prostate biopsy, The Journal of urology 188(6) (2012) 2404–2409. [PubMed: 23088974]

[3]. Hricak H, Choyke PL, Eberhardt SC, Leibel SA and Scardino PT, Imaging prostate cancer: A multidisciplinary perspective 1, Radiology 243(1) (2007) 28–53. [PubMed: 17392247]

[4]. Xu S, Kruecker J, Turkbey B, Glossop N, Singh AK, Choyke P, Pinto P and Wood BJ, Real-time mri-trus fusion for guidance of targeted prostate biopsies, Computer Aided Surgery 13(5) (2008) 255–264. [PubMed: 18821344]

[5]. Kadoury S, Yan P, Xu S, Glossop N, Choyke P, Turkbey B, Pinto P, Wood BJ and Kruecker J, Realtime trus/mri fusion targeted-biopsy for prostate cancer: a clinical demonstration of increased positive biopsy rates, International Workshop on Prostate Cancer Imaging, Springer (2010), pp. 52–62.

[6]. Thoma C, Prostate cancer: Mri/trus fusion outperforms standard and combined biopsy approaches, Nature Reviews Urology 12(3) (2015) 119–119.

[7]. Susil RC, Mard C, Krieger A, Coleman JA, Camphausen K, Choyke P, Fichtinger G, Whitcomb LL, Coleman CN and Atalar E, Transrectal prostate biopsy and fiducial marker placement in a standard 1.5t magnetic resonance imaging scanner., J Urol 175 (1 2006) 113–120. [PubMed: 16406885]

[8]. Beyersdorff D, Winkel A, Hamm B, Lenk S, Loening SA and Taupitz M, Mr imaging-guided prostate biopsy with a closed mr unit at 1.5 t: Initial results 1, Radiology 234(2) (2005) 576–581. [PubMed: 15616117]

[9]. D'Amico AV, Tempany CM, Cormack R, Hata N, Jinzaki M, Tuncali K, Weinstein M and Richie JP, Transperineal magnetic resonance image guided prostate biopsy., J Urol 164 (8 2000) 385–387. [PubMed: 10893591]

[10]. Penzkofer T, Tuncali K, Fedorov A, Song S-E, Tokuda J, Fennessy FM, Vangel MG, Kibel AS, Mulkern RV, Wells WM et al., Transperineal in-bore 3-t mr imaging-guided prostate biopsy: A prospective clinical observational study, Radiology 274(1) (2014) 170–180. [PubMed: 25222067]

[11]. Fischer GS, Iordachita I, Csoma C, Tokuda J, DiMaio SP, Tempany CM, Hata N and Fichtinger G, MRI- compatible pneumatic robot for transperineal prostate needle placement, IEEE/ASME Transactions on Mechatronics 13(3) (2008).

[12]. Song S-E, Hata N, Iordachita I, Fichtinger G, Tempany C and Tokuda J, A workspace-orientated needle-guiding robot for 3t mri-guided transperineal prostate intervention: evaluation of in-bore workspace and mri compatibility, The International Journal of Medical Robotics and Computer Assisted Surgery 9(1) (2013) 67–74. [PubMed: 22492680]

[13]. Van den Bosch MR, Moman MR, Van Vulpen M, Battermann JJ, Duiveman E, van Schelven LJ, de Leeuw H, Lagendijk JJ and Moerland MA, Mri-guided robotic system for transperineal prostate interventions: proof of principle, Physics in medicine and biology 55(5) (2010) p. N133. [PubMed: 20145293]

[14]. Zemiti N, Bricault I, Fouard C, Sanchez B and Cinquin P, Lpr: A ct and mr-compatible puncture robot to enhance accuracy and safety of image-guided interventions, IEEE/ASME Transactions on Mechatronics 13(3) (2008) 306–315.

[15]. Stoianovici D, Kim C, Srimathveeravalli G, Sebrecht P, Petrisor D, Coleman J, Solomon SB and Hricak H, MRI-safe robot for endorectal prostate biopsy, IEEE/ASME Transactions on Mechatronics (99) (2013) 1–11.

[16]. Stoianovici D, Song D, Petrisor D, Ursu D, Mazilu D, Muntener M, Mutener M, Schar M and Patriciu A, MRI Stealth robot for prostate interventions., Minim Invasive Ther Allied Technol 16(4) (2007) 241–248. [PubMed: 17763098]

[17]. Chen Y, Mershon CD and Tse ZTH, A 10-mm mr-conditional unidirectional pneumatic stepper motor, IEEE/ASME Transactions on Mechatronics 20(2) (2015) 782–788. [PubMed: 25419104]

[18]. Schouten MG, Ansems J, Renema WKJ, Bosboom D, Scheenen TW and Fiitterer JJ, The accuracy and safety aspects of a novel robotic needle guide manipulator to perform transrectal prostate biopsies, Medical physics 37(9) (2010) 4744–4750. [PubMed: 20964192]

[19]. Zangos S, Melzer A, Eichler K, Sadighi C, Thalhammer A, Bodelle B, Wolf R, Gruber-Rouh T, Proschek D, Hammerstingl R et al., Mr-compatible assistance system for biopsy in a high-field-strength system: initial results in patients with suspicious prostate lesions, Radiology 259(3) (2011) 903–910. [PubMed: 21364080]

[20]. Song S-E, Tokuda J, Tuncali K, Tempany CM, Zhang E and Hata N, Development and preliminary evaluation of a motorized needle guide template for mri-guided targeted prostate biopsy, Biomedical Engineering, IEEE Transactions on 60(11) (2013) 3019–3027.

[21]. Krieger A, Song S-E, Cho NB, Iordachita II, Guion P, Fichtinger G and Whitcomb LL, Development and evaluation of an actuated mri-compatible robotic system for mri-guided prostate intervention, Mechatronics, IEEE/ASME Transactions on 18(1) (2013) 273–284.

[22]. Fischer GS, Krieger A, Iordachita I, Csoma C, Whitcomb LL and Fichtinger G, MRI compatibility of robot actuation techniques - a comparative study, Int Conf Med Image Comput Comput Assist Interv (Sept. 2008).

[23]. Li G, Su H, Cole G, Shang W, Harrington K, Camilo A, Pilitsis JG, Fischer GS et al., Robotic system for mri-guided stereotactic neurosurgery, Biomedical Engineering, IEEE Transactions on 62(4) (2015) 1077–1088.

[24]. Su H, Shang W, Cole G, Li G, Harrington K, Camilo A, Tokuda J, Tempany CM, Hata N and Fischer GS, Piezoelectrically actuated robotic system for mri-guided prostate percutaneous therapy, IEEE/ASME Transactions on Mechatronics 20(4) (2015) 1920–1932. [PubMed: 26412962]

[25]. Li G, Su H, Shang W, Tokuda J, Hata N, Tempany CM and Fischer GS, A fully actuated robotic assistant for mri-guided prostate biopsy and brachytherapy, SPIE Medical Imaging, International Society for Optics and Photonics (2012), pp. 867117–867117.

[26]. Stoianovici D, Kim C, Petrisor D, Jun C, Lim S, Ball M, Ross A, Macura K and Allaf M, Mr safe robot, fda clearance, safety and feasibility prostate biopsy clinical trial, IEEE/ASME Transactions on Mechatronics (2016).

[27]. Tilak G, Tuncali K, Song S-E, Tokuda J, Olubiyi O, Fennessy F, Fedorov A, Penzkofer T, Tempany C and Hata N, 3t mr-guided in-bore transperineal prostate biopsy: A comparison of robotic and manual needle-guidance templates, Journal of Magnetic Resonance Imaging (2014).

[28]. Yakar D, Schouten MG, Bosboom DG, Barentsz JO, Scheenen TW and Fiitterer JJ, Feasibility of a pneumatically actuated mr-compatible robot for transrectal prostate biopsy guidance, Radiology 260(1) (2011) 241–247. [PubMed: 21406625]

[29]. Elhawary H, Tse ZTH, Hamed A, Rea M, Davies BL and Lamperth MU, The case for MR-compatible robotics: a review of the state of the art, The international journal of medical robotics and computer assisted surgery 4(2) (2008) 105–113. [PubMed: 18481822]

[30]. Fiitterer JJ, Misra S and Macura KJ, MRI of the prostate: potential role of robots, Imaging 2(5) (2010) 583–592.

[31]. Gassert R, Yamamoto A, Chapuis D, Dovat L, Bleuler H and Burdet E, Actuation methods for applications in mr environments, Concepts in Magnetic Resonance Part B: Magnetic Resonance Engineering 29(4) (2006) p. 191.

[32]. Tokuda J, Song S-E, Fischer G, Iordachita I, Seifabadi R, Cho N, Tuncali K, Fichtinger G, Tempany C and Hata N, Preclinical evaluation of an mri-compatible pneumatic robot for angulated needle placement in transperineal prostate interventions, International Journal of Computer Assisted Radiology and Surgery 7 (2012) 949–957. [PubMed: 22678723]

[33]. Eslami S, Shang W, Li G, Patel N, Fischer GS, Tokuda J, Hata N, Tempany CM and Iordachita I, In-bore prostate transperineal interventions with an mri-guided parallel manipulator: system development and preliminary evaluation, The International Journal of Medical Robotics and Computer Assisted Surgery (2015).

[34]. Fedorov A, Beichel R, Kalpathy-Cramer J, Finet J, Fillion-Robin J-C, Pujol S, Bauer C, Jennings D, Fen- nessy F, Sonka M et al., 3d slicer as an image computing platform for the quantitative imaging network, Magnetic resonance imaging 30(9) (2012) 1323–1341. [PubMed: 22770690]

[35]. Fedorov A, Tuncali K, Fennessy FM, Tokuda J, Hata N, Wells WM, Kikinis R and Tempany CM, Image registration for targeted mri-guided transperineal prostate biopsy, Journal of Magnetic Resonance Imaging 36(4) (2012) 987–992. [PubMed: 22645031]

[36]. Tokuda J, Fischer GS, Papademetris X, Yaniv Z, Ibanez L, Cheng P, Liu H, Blevins J, Arata J, Golby AJ et al., Openigtlink: an open network protocol for image-guided therapy environment, The International Journal of Medical Robotics and Computer Assisted Surgery 5(4) (2009) 423–434. [PubMed: 19621334]

[37]. Tokuda J, Tuncali K, Iordachita I, Song S-E, Fedorov A, Oguro S, Lasso A, Fennessy FM, Tempany CM and Hata N, In-bore setup and software for 3t mri-guided transperineal prostate biopsy, Physics in medicine and biology 57(18) (2012) p. 5823. [PubMed: 22951350]

[38]. Tokuda J, Song S-E, Tuncali K, Tempany C and Hata N, Configurable automatic detection and registration of fiducial frames for device-to-image registration in mri-guided prostate interventions, Medical Image Computing and Computer-Assisted Intervention-MICCAI 2013, (Springer, 2013), pp. 355–362.

[39]. Hungr N, Bricault I, Cinquin P and Fouard C, Design and validation of a ct-and mri-guided robot for percutaneous needle procedures, IEEE Transactions on Robotics 32(4) (2016) 973–987.

[40]. Patel N, van KatwijK T, Li G, Moreira P, Shang W, Misra S and Fischer G, Closed-loop asymmetric-tip needle steering under continuous intraoperative mri guidance, Annual Conference of IEEE Engineering in Medicine and Biology Society, (2015).

[41]. Su H, Li G, Rucker DC, Webster III RJ and Fischer GS, A concentric tube continuum robot with piezoelectric actuation for mri-guided closed-loop targeting, Annals of biomedical engineering 44(10) (2016) 2863–2873. [PubMed: 26983842]

[42]. Code of federal regulations. title 21. food and drugs. chapter i-food and drug administration. department of health and human services subchapter h. medical devices. part 812. investigational device exemptions.

[43]. Ploussard G, Epstein JI, Montironi R, Carroll PR, Wirth M, Grimm M-O, Bjartell AS, Montorsi F, Freedland SJ, Erbersdobler A et al., The contemporary concept of significant versus insignificant prostate cancer, European urology 60(2) (2011) 291–303. [PubMed: 21601982]

[44]. Shang W, Su H, Li G and Fischer GS, Teleoperation system with hybrid pneumatic-piezoelectric actuation for mri- guided needle insertion with haptic feedback, Intelligent Robots and Systems (IROS), 2013 IEEE/RSJ International Conference on, IEEE (2013), pp. 4092–4098.

[45]. Li M, Gonenc B, Kim K, Shang W and Iordachita I, Development of an mri-compatible needle driver for in-bore prostate biopsy, 17th International Conference on Advanced Robotics, ICAR, (2015).
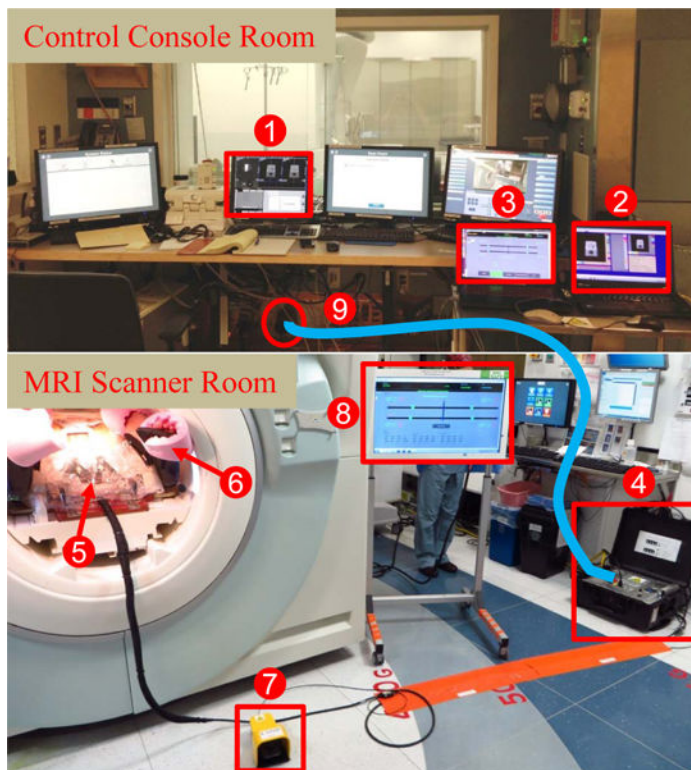
Fig. 1.
Clinical system configuration. In the control console room: (1) MRI scanner control, (2) surgical navigation user interface, and (3) robot control software. Inside the scanner room: (4)robot controller, (5) robotic manipulator inside the scanner bore covered with sterile drape, (6) patient lying inside the scanner bore in semi-lithotomy position, (7) fiberoptic foot-pedal interlock, and (8)display showing robot status to the clinician in the scanner room. Communication between the control room and scanner room is through (9) fiber optic cable.
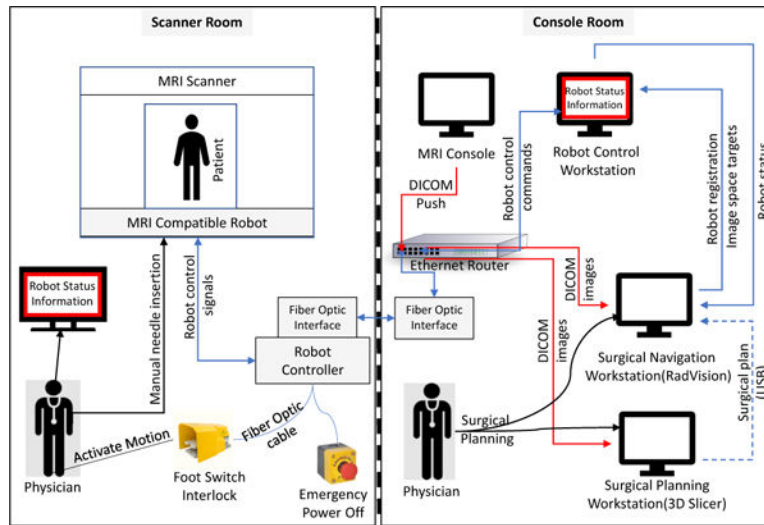
Fig. 2.
System block diagram showing integration of all components and data flow between them. The robot status information display inside the scanner room is connected to the robot control workstation through the scanner console display system.
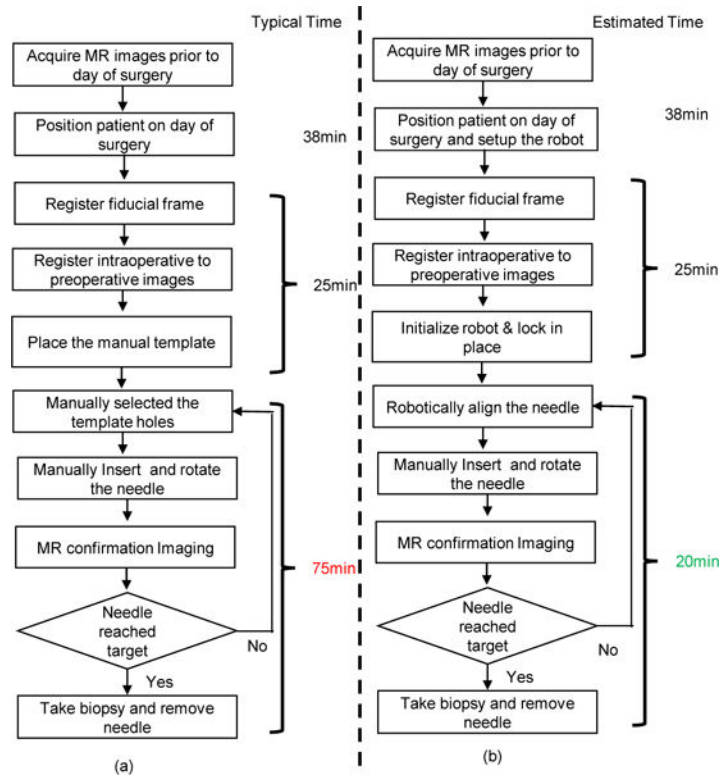
Fig. 3.

Workflow comparison of manual template-based approach and robot-assisted approach for MRI-guided prostate biopsy. (a) Workflow of a manual template-based prostate biopsy with measured average time per step. (b) Workflow of a robot-assisted prostate biopsy with estimated time per step.
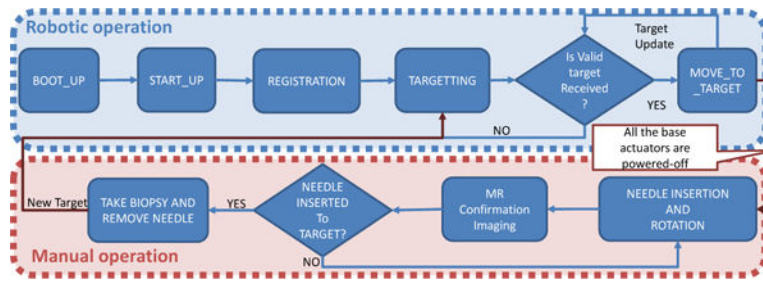
Fig. 4.
Flowchart of the robot control workflow and robot operation modes, showing only valid transitions from one state to another.
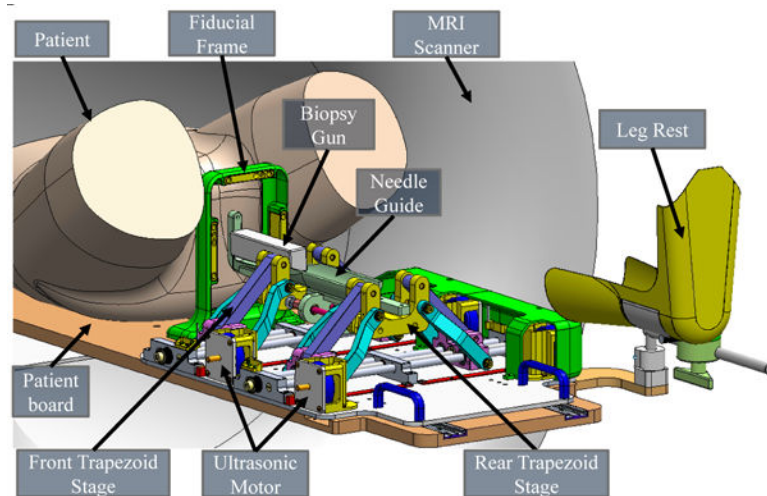
Fig. 5.
Annotated CAD model of the parallel manipulator for transperineal prostate intervention inside the MRI scanner bore. The patient lies in the supine position, the robotic manipulator is placed between the legs, and a biopsy gun targets the prostate through the perineum. Note that the leg rest and motor covers are hidden on the left side to visualize the internal structure of the manipulator.
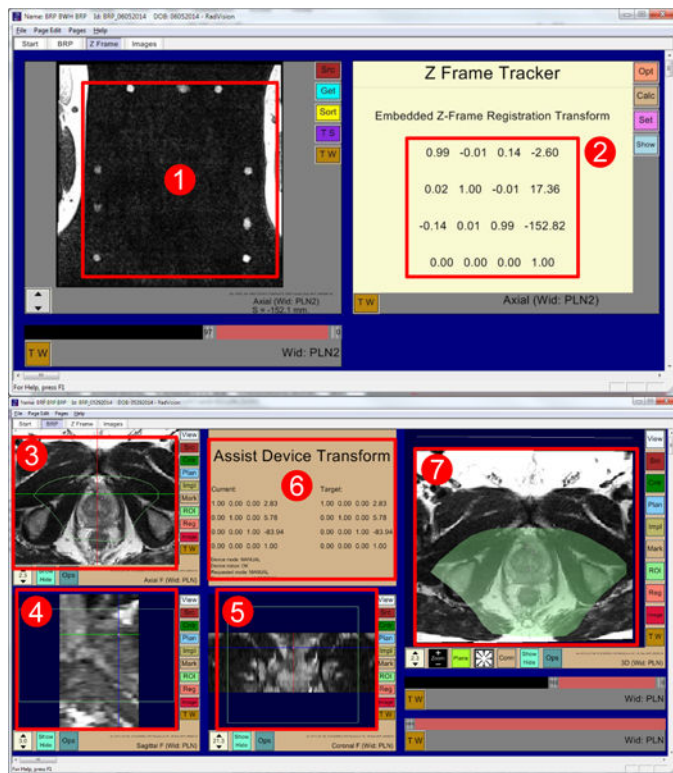
Fig. 6.

RadVision user interface showing (1) acquired MR images of fiducial frame, (2) calculated robot registration transform, (3) axial view, (4) sagittal view, (5) coronal view, (6) robot status, current robot pose, and desired target pose, and (7) 3D view with overlaid reachable robot workspace shown in light green. Also in all image views (3, 4, 5) light green boundary indicates reachable robot workspace.
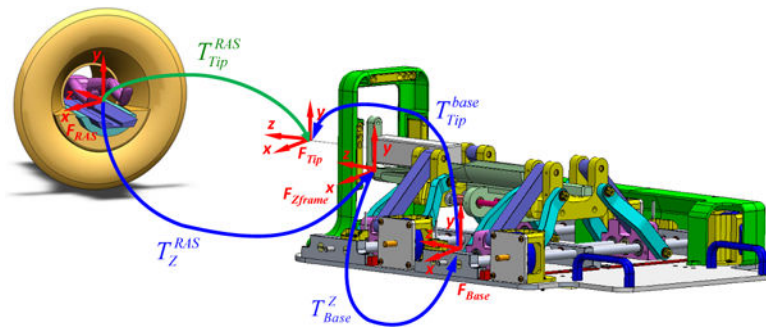
Fig. 7.
Kinematic transformation chain for registering the robotic system to the MR scanner coordinate system (RAS coordinates) based on imaging of the fiducial frame (Z-Frame).
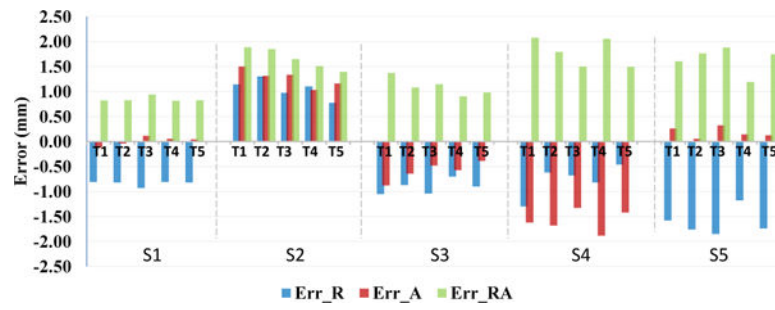
Fig. 8.

Phantom studies accuracy assessment: plot of measured needle placement accuracy in each of the five trials in each of the five sessions. Data is shown with errors in the lateral R-L direction (*Err_R*), vertical A-P direction (*Err_A*), and total in-plane error magnitude (*Err_RA*).
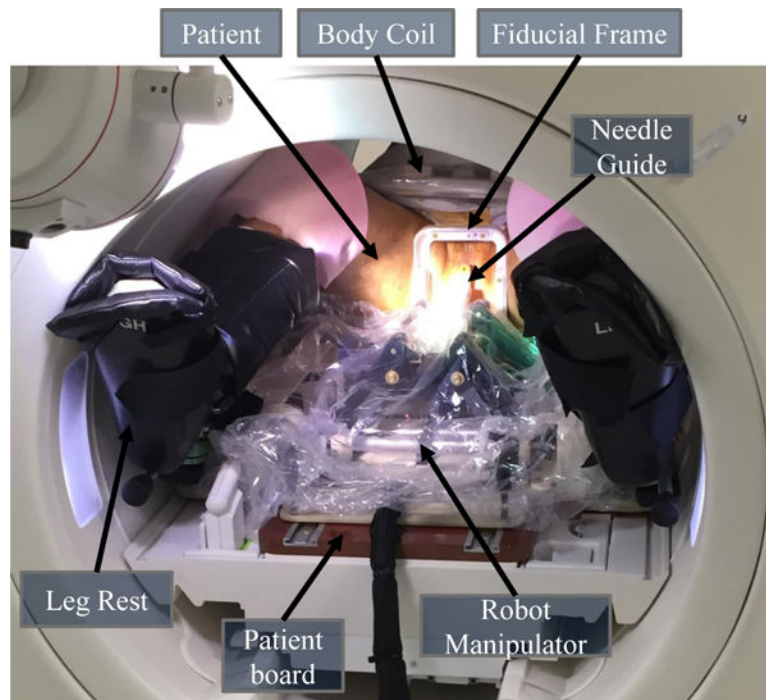
Fig. 9.
System configuration for the patient study. The patient lies in the supine position with legs supported by the leg rest on the patient board. The sterilized fiducial frame is fixed to the patient board between the patient's legs. The robot manipulator is covered by the sterile plastic drape with sterile needle guide affixed, positioned on the patient board, and locked into place.
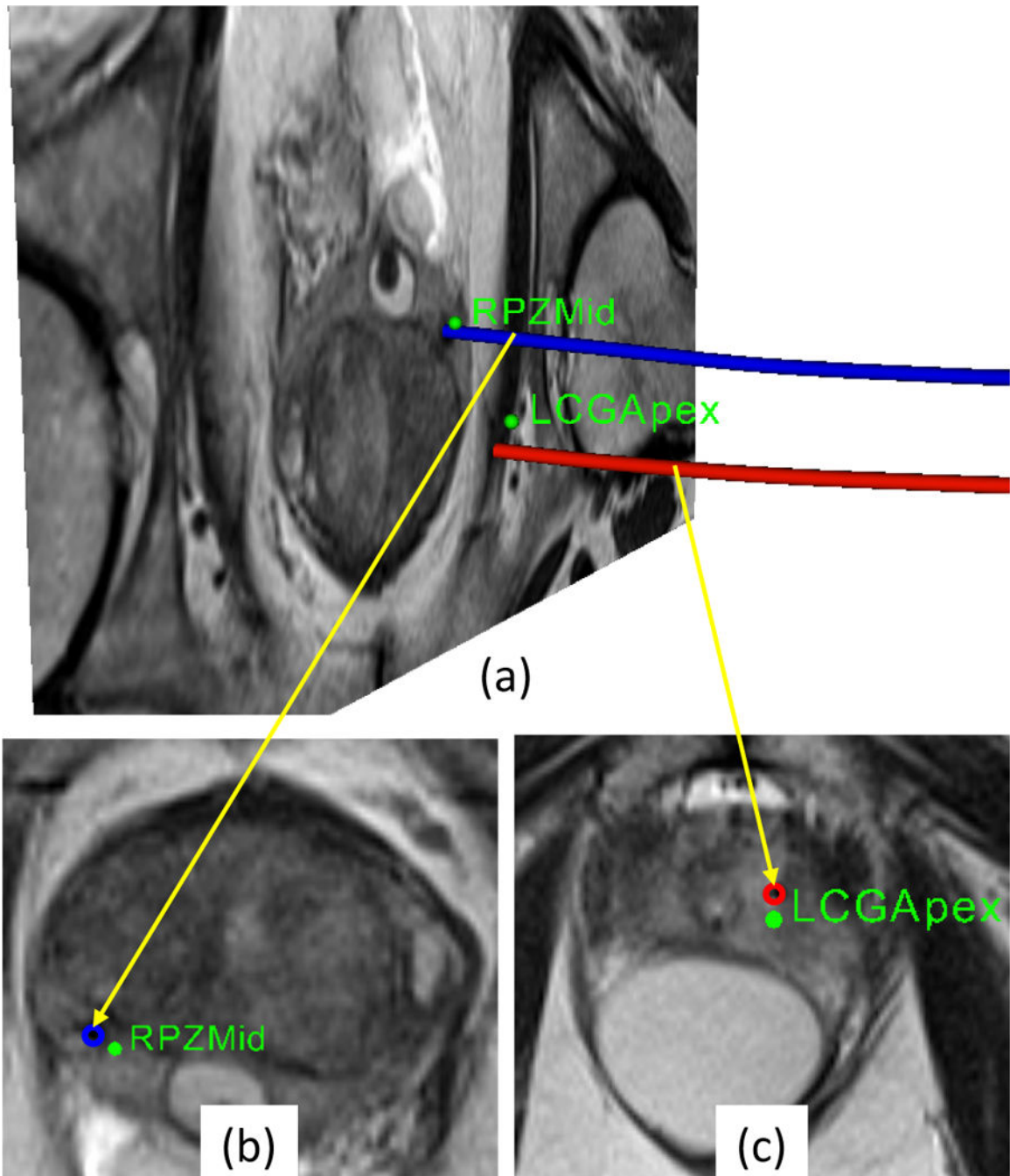
Fig. 10.
(a)Snapshot of 3D view with an MR image of prostate gland showing desired targets (green spheres) and actual needle trajectories segmented from the MRI volume images, (b-c)zoomed-in view of transverse image slice showing targets and intersection of the image slice with corresponding needle trajec- tories(the blue and red circles) from the confirmation images.

Table 1.

Experimental Results of MRI Phantom Study

Session #	Error$_R$(mm)			Error$_{RA}$(mm)			ErrorRv(mm)		
	along R axis			along A axis			in R-A plane		
	Max	Min	RMS	Max	Min	RMS	Max	Min	RMS
1	−0.9	−0.8	0.8	−0.1	0.1	0.1	0.9	0.8	0.8
2	1.3	0.8	1.1	1.5	1	1.3	1.9	1.4	1.7
3	−1.1	−0.7	0.9	−0.9	−0.4	0.6	1.4	0.9	1.1
4	−1.3	−0.5	0.8	−1.9	−1.3	1.6	2.1	1.5	1.8
5	−1.9	−1.2	1.6	0.3	0.1	0.2	1.9	1.2	1.7
Total			1.1			1			1.5

Table 2.

Imaging Protocols for the Phantom and Patient Study

Imaging Protocol	Localizer	Intraoperative	Needle Confirmation
Sequence	T2W-TSE	T2W-TSE	T2W-TSE
Flip Angle(deg)	120	150	120
TR(ms)	3000	4800	3000
TE(ms)	111	100	106
Slice Thickness (mm)	2	3	3
Pixel Spacing(mm x mm)	0.70×0.70	0.70×0.70	0.70×0.70
Scan Time(mm:ss)	01:44	03:04	00:31

Table 3.

Experiment Results of Patient Study

Target	Target Position (mm)			First Attempt Error (mm)				Best Attempt Error (mm)			
	R	A	S	R	A	S	Total	R	A	S	Total
LCGApex	−13.2	8.5	15.6	−5.8	7.7	−1.1	9.7	−0.4	4	0.1	4
RPZMid	8.8	0	33.6	0	6.3	0	6.3	3.1	2	−0.3	3.7